Dynamics of phase transitions in a piecewise linear diatomic chain

Anna Vainchtein * Panayotis G. Kevrekidis †

September 22, 2011

Abstract

We consider a diatomic chain with nearest neighbors connected by phase transforming springs. Assuming a piecewise linear interaction force, we use Fourier transform to construct exact traveling wave solutions representing a moving phase transition front and examine their stability through numerical experiments. We find that the identified traveling wave solutions may be stable in some velocity intervals. We show that the kinetic relation between the driving force on the phase boundary and its velocity is significantly affected by the ratio of the two masses. When the ratio is small enough, the relation may become multivalued at some velocities, with the two solutions corresponding to the different orders in which the two springs in a dimer cell change phase. The model bears additional interesting waveforms such as the so-called twinkling phase, which is also briefly touched upon and compared to its monatomic analog.

1 Introduction

The examination of coupled nonlinear oscillators has a long history, originating with the Fermi-Pasta-Ulam problem [8, 19]. In recent years, it is

*Department of Mathematics, University of Pittsburgh, Pittsburgh, PA 15260, aav4@pitt.edu

†Department of Mathematics and Statistics, University of Massachusetts, Amherst, MA 01003, kevrekid@math.umass.edu

maturing as a field with numerous areas of application ranging from coupled waveguide arrays and photorefractive crystals in nonlinear optics [22, 15] to Bose-Einstein condensates in optical lattices in atomic physics [30], and from DNA double-strand dynamics in biophysics [32] to ferromagnetic or nanomechanical systems [35]. A topic of particular interest within this broader subject has often been the study of heterogeneous environments versus uniform nonlinear lattices. An arguably prototypical example of a heterogeneous dynamical lattice has been that of dimers, i.e. chains consisting of two alternating materials (in the simplest possible implementation two different masses). Studies of diatomic lattices with harmonic interactions date back to the work of Kelvin that led to the design of the first mechanical filter [7]. In the nonlinear case, the dimer setting has attracted considerable attention in its own right, with applications ranging from ferroelectric perovskites [5] and polymers [33] to optical waveguides [42], granular crystals [6] and cantilever arrays [35].

On the other hand, models with piecewise linear nonlinearity have been used to understand a wide array of nonlinear phenomena, including breather solutions of discrete nonlinear Schrödinger and Klein-Gordon equations [25] and dynamics of dislocations [2, 10, 11, 13, 18, 17, 20, 23, 50, 52, 53], shock waves [41, 43], fracture [28, 37, 38] and phase transitions [3, 4, 24, 39, 40, 43, 47, 46, 48, 49, 51] in monatomic crystal lattices (see also the references therein). The notable advantage of this approach is that the piecewise linear nature of the nonlinearity makes it possible to construct explicit traveling wave solutions using Fourier transform techniques. Although they lead to a non-generic asymptotic behavior near the depinning threshold [14, 9], piecewise linear models capture the main features observed numerically in the fully nonlinear case, including lattice trapping and radiative damping due to phonons emitted by the moving defects in a Hamiltonian lattice. In the diatomic setting, this approach has been used to show that the ratio of the two masses has a substantial effect on the dynamics of dislocation in a Frenkel-Kontorova chain [16] and crack propagation in a heterogeneous two-dimensional lattice [29].

In the present communication we combine these two themes, a dimer setting and a piecewise linear nonlinearity, to study the dynamics of phase transitions. We consider a chain of two alternating masses connected by "snap-springs" that are governed by a piecewise linear interaction force. The two linear regimes correspond to two different material phases. The monatomic case was studied in [3, 4, 39, 40] and in [47, 46], where interac-

tions beyond nearest neighbors were also included, and the present study is a natural extension of that work. It can also be viewed as an extension of the semilinear problem considered in [16] for the diatomic chain with harmonic nearest-neighbor interactions and nonlinear onsite potential to the present quasilinear setting, where the forces in the nearest-neighbor springs are nonlinear. Our goal is to gain some insight into how heterogeneity of the lattice, common in phase transforming materials and modeled here by a diatomic chain, affects the phase boundary dynamics.

To study kinetics of a phase boundary, we rewrite the problem as a two-strain formulation and seek heteroclinic traveling wave solutions connecting the equilibrium states in different wells of the biquadratic interaction potential and representing a moving phase boundary. As in the previous work, this leads to a system of linear advance-delay differential equations for even and odd strains, which is solved using Fourier transform. The main parameter in the problem is the ratio λ of the two masses, $0 < \lambda \leq 1$, with $\lambda = 1$ corresponding to the monomer case studied earlier and $\lambda \to 0$ corresponding to one of the masses being much heavier than the other. As in [16], a new element introduced by the dimer setting ($\lambda < 1$) is the difference, measured by the variable α, between the times two springs switch phases in a dimer cell. The values of α and the corresponding values of the driving force G for the given value of the phase boundary velocity are determined by the nonlinear phase switch conditions and the assumed phase distribution inequalities. We show that at small enough λ, there can be at least two values of α in some velocity intervals, corresponding to two modes of phase propagation at the same average velocity. In one mode, $\alpha > 0$, the two springs in a dimer cell switch phase consecutively, while in the other, $\alpha < 0$, the second spring in each cell changes phase first. The latter propagation mode corresponds to a new type of solution, which has no analog in the monatomic setting. The coexistence of the two propagation modes results in a multivalued kinetic relation between the driving force and phase boundary velocity. We also find that at smaller λ a higher driving force is required for a phase boundary to move with a given speed due to the weaker coupling between the neighboring dimer cells. Numerical simulations with piecewise constant and smooth initial data verify the analytical results and suggest stability of the obtained solutions in certain ranges of sufficiently high velocities. At intermediate values of λ, this includes coexisting solutions with positive and negative values of α and the same velocity. Overall, our results demonstrate that lattice heterogeneity may substantially affect phase boundary kinetics.

While the main focus of this work is on traveling phase transition fronts, other interesting wave forms in this system may develop under different initial conditions. A prototypical one among them is the so-called twinkling phase, analyzed in the monomer case of $\lambda = 1$ in [3, 4]. Here, we illustrate that an analog of this phase persists for $\lambda < 1$, although it becomes progressively less ordered as λ decreases.

The paper is organized as follows. In Section 2 below, we set up the dimer model with piecewise linear interactions, rewrite it in the corresponding two-strain formulation and obtain the system of advance-delay differential equations for the traveling phase transition wave. In Section 3, we proceed to take advantage of the near-linear character of the model to solve these equations using Fourier transform. As a result, the roots of the underlying linear operator (in the co-traveling frame) become of interest. Upon connecting the problem to its corresponding continuum limit in Section 4, we proceed to examine the structure of these roots, which is more complex in the diatomic setting, in more detail in Section 5. In Section 6, we use the above approach to explicitly construct traveling wave solutions which through their resonance with the linear modes include different plane waves in the tail behind the moving front. Stability of the waves is investigated through numerical simulations in Section 7. Finally, in Section 8, a prototypical example of alternative wave profiles forming spontaneously through suitable initial data (and its variation over λ) is given. Section 9 concludes the paper and offers some suggestions for future study. In the Appendix, explicit solutions are derived using the residue theorem.

2 The model

We consider in what follows a chain of alternating masses, m and $M \geq m$, connected by massless springs with the interaction force $f(w)$. Let $u_n(t)$ and $v_n(t)$ denote the displacements of the masses m and M, respectively (see Fig. 1). Then the equations governing the dynamics of the chain are

$$\begin{aligned} m\ddot{u}_n &= f(v_{n+1} - u_n) - f(u_n - v_n) \\ M\ddot{v}_n &= f(u_n - v_n) - f(v_n - u_{n-1}), \end{aligned} \tag{1}$$

where $\ddot{u}_n$ and $\ddot{v}_n$ denote the second time derivatives. It is convenient to rewrite the problem in terms of strain variables

$$r_n = u_n - v_n, \quad s_n = v_{n+1} - u_n;$$

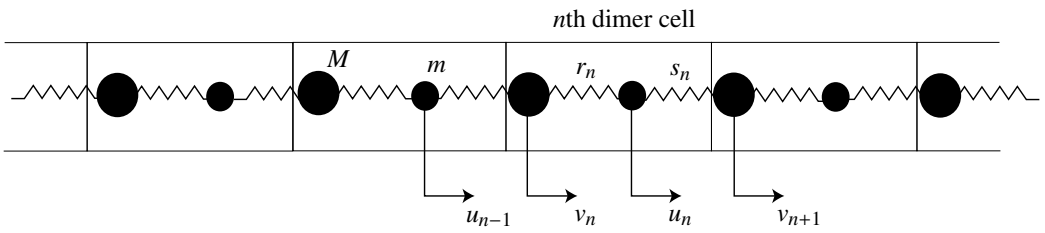

Figure 1: The diatomic chain.

the pair of strains (r_n, s_n) then describes deformation inside the nth dimer cell (see Fig. 1). In terms of these variables, the equations of motion become

$$\begin{aligned}\ddot{r}_n &= \frac{1}{m}f(s_n) - \frac{m+M}{mM}f(r_n) + \frac{1}{M}f(s_{n-1})\\ \ddot{s}_n &= \frac{1}{M}f(r_{n+1}) - \frac{m+M}{mM}f(s_n) + \frac{1}{m}f(r_n).\end{aligned}$$

Let $K > 0$ be the scale of force (that can be selected upon rescaling convenience) and introduce the rescaled force $\bar{f} = f/K$ and time $\bar{t} = t\sqrt{m/K}$. After dropping the bars, we obtain the rescaled equations

$$\begin{aligned}\ddot{r}_n &= f(s_n) - (1+\lambda)f(r_n) + \lambda f(s_{n-1})\\ \ddot{s}_n &= \lambda f(r_{n+1}) - (1+\lambda)f(s_n) + f(r_n),\end{aligned} \tag{2}$$

where we introduced the dimensionless parameter

$$\lambda = \frac{m}{M}. \tag{3}$$

Note that under our assumptions $0 \le \lambda \le 1$. At $\lambda = 1$ the problem reduces to the one for monatomic chain. The case of $\lambda = 0$ also provides an interesting special limit. In this case, the dimer cells decouple, i.e. the strain pair (r_n, s_n) no longer "communicates" with the neighboring pairs (r_{n-1}, s_{n-1}) and (r_{n+1}, s_{n+1}), and we end up with a lattice of isolated dimer cells. In the case of special localized breathing solutions [27, 21], this can be used as a starting point for the development of nontrivial solutions of this type through a continuation in λ. However, for the traveling solutions considered herein, such a decoupling is less beneficial; in fact, some of its adverse consequences will become apparent in our dynamical studies in Sections 7 and 8. For these reasons, we will not attempt to exploit this limit in the present work.

To model phase transitions, we assume that $f(w)$ is a non-monotone function such that $f'(w) > 0$ for $w < a$ and $w > b$, for some a and b satisfying $0 < a < b$, and $f'(w) < 0$ for $a < w < b$. The two regions where $f(w)$ is increasing represent two different phases and are separated by the spinodal region (a, b). The motion of a phase transition front can then be represented by a traveling wave solution of (2) of the form

$$r_n = r(\xi), \quad s_n = s(\xi), \quad \xi = n - ct \tag{4}$$

that connects equilibrium states in two different phases. Here $c > 0$ is half of the velocity $V = 2c$ of the moving phase boundary. Such solutions must satisfy the advance-delay equations

$$\begin{aligned} c^2 r'' &= f(s(\xi)) - (1+\lambda) f(r(\xi)) + \lambda f(s(\xi - 1)) \\ c^2 s'' &= \lambda f(r(\xi + 1)) - (1+\lambda) f(s(\xi)) + f(r(\xi)). \end{aligned} \tag{5}$$

An exact solution of this problem can be obtained if we assume that $f(w)$ is bilinear:

$$f(w) = w - \theta(w - w_c), \tag{6}$$

where $\theta(x)$ is a unit step function. In this case, $a = b = w_c$, and the spinodal region degenerates into a single point $w = w_c$ separating the two phases where $f(w)$ is linear: phase I ($w < w_c$) and phase II ($w > w_c$). Without loss of generality we may assume that the r-springs change phases at $\xi = 0$, while the s-springs switch at $\xi = -\alpha$, where α is to be determined:

$$r(0) = s(-\alpha) = w_c. \tag{7}$$

We further assume that the moving phase boundary leaves the high-strain phase II behind, i.e.

$$r(\xi) \gtrless w_c, \quad \xi \lessgtr 0, \qquad s(\xi) \gtrless w_c, \quad \xi \lessgtr -\alpha. \tag{8}$$

To find the limits of the delay constant α, let $w_p(t)$ denote the strain in pth nearest-neighbor spring and consider the nth dimer cell, which includes two consecutive springs with strains $w_{2n}(t) = r(n - ct)$ and $w_{2n+1}(t) = s(n - ct)$ (see Fig. 1). By construction, the first spring in the cell switches from phase I to phase II at $t = n/c$, and the second changes phase at $t = (n + \alpha)/c$. Thus $\alpha > 0$ means that the second spring changes phase *after* the first, $\alpha = 0$ corresponds to both springs changing phase simultaneously, and $\alpha < 0$ means

that the second spring switches to phase II *before* the first spring. We consider a phase transition wave in which the dimer cells transform consecutively, so that the time delay between phase switch in the first and second springs in a cell may not exceed $1/c$, the time between transformations of first (second) springs in the neighboring dimers. Thus we have

$$-1 < \alpha < 1. \tag{9}$$

Under the above assumptions, the system (5) becomes

$$\begin{aligned} c^2 r'' &= s(\xi) - (1+\lambda) r(\xi) + \lambda s(\xi - 1) + (1+\lambda)\theta(-\xi) - \theta(-\xi - \alpha) - \lambda\theta(1 - \alpha - \xi) \\ c^2 s'' &= \lambda r(\xi + 1) - (1+\lambda) s(\xi) + r(\xi) + (1+\lambda)\theta(-\xi - \alpha) - \lambda\theta(-\xi - 1) - \theta(-\xi). \end{aligned} \tag{10}$$

We need to solve (10) under the switch condition (7), the constraints (8) and the conditions at infinity

$$\langle r \rangle,\ \langle s \rangle \longrightarrow w_{\pm} \quad \text{as } \xi \to \pm\infty, \tag{11}$$

where the angular brackets denote the average values. Here the average is taken over the largest period of oscillations that we expect to develop in the Hamiltonian system (10) but can also be defined as $\langle w(\xi) \rangle = \lim_{p\to\infty} \int_{\xi}^{\xi+p} w(\zeta) d\zeta$. The limiting average strains w_+ and w_- are the uniform equilibrium states of (10) in phase I and phase II, respectively.

3 Exact solution

Since the system (10) is linear, we can solve it using Fourier transform. We obtain

$$\begin{aligned} r(\xi) =& w_+ + \frac{1}{2\pi i} \int_{\Gamma} \frac{c^2 k^2 (\lambda + 1 - e^{(\alpha-1)ik}(\lambda + e^{ik})) - 4\lambda \sin^2 \frac{k}{2}}{k \mathcal{L}(k, c)} e^{ik\xi} dk \\ s(\xi) =& w_+ + \frac{1}{2\pi i} \int_{\Gamma} \frac{c^2 k^2 (\lambda + 1 - e^{(1-\alpha)ik}(\lambda + e^{-ik})) - 4\lambda \sin^2 \frac{k}{2}}{k \mathcal{L}(k, c)} e^{ik(\xi+\alpha)} dk, \end{aligned} \tag{12}$$

where

$$\mathcal{L}(k, c) = c^4 k^4 + 4\lambda \sin^2 \frac{k}{2} - 2(1+\lambda) c^2 k^2 \tag{13}$$

and the integration contour Γ follows the real axis except near singularities (poles in the complex plane). One such singularity is at $k = 0$, and the contour goes above it. There is also a finite number of nonzero real roots of $\mathcal{L}(k, c)$ which correspond to lattice waves emitted by the moving front. As in [23, 47], these singularities must be handled so that the solution satisfies the radiation condition: waves must carry energy away from the moving front and not toward it. Specifically, let $\omega(k)$ be the dispersion relation between the frequency of the plane wave and its wave number k; positive real roots of $L(k, c)$ satisfy $\omega(k) = kc$, meaning that c is the phase velocity. Note that in the diatomic case $\lambda < 1$ the dispersion curve has two branches, the acoustic branch $\omega_1(k)$ and the optical branch $\omega_2(k)$ given by

$$\omega_{1,2}(k) = \left(\lambda + 1 \mp \sqrt{(\lambda+1)^2 - 4\lambda \sin^2(k/2)}\right)^{1/2},$$

with $\omega_2(k) > \omega_1(k)$ [7]. The radiation condition means that waves whose group velocity $c_g = \omega'(k)$ is below the phase velocity c must propagate behind the front, while the modes with $c_g > c$ are placed ahead of it; in what follows, we denote the corresponding sets of nonzero real roots of (13) by N_- and N_+, respectively. To ensure that the radiation condition is satisfied, the contour Γ must go above the real roots with $c_g < c$ and below the roots with $c_g > c$.

In what follows, we will assume $0 < \lambda < 1$; the limiting case $\lambda = 1$ obtained in [39, 47] will be recovered at the end of the section. We start by deriving the equation for the delay constant α for given $c > 0$. Observe that the condition $r(0) - s(-\alpha) = 0$, which follows from (7), and (12) implies that α must be a solution of $f(\alpha) = 0$, where

$$f(\alpha) = \frac{1}{\pi} \int_\Gamma k \frac{\lambda \sin(k(1-\alpha)) - \sin(k\alpha)}{\mathcal{L}(k, c)} dk. \tag{14}$$

Observe that $f(0) = -\lambda f(1)$, and thus there exists at least one root satisfying $0 \le \alpha < 1$. Indeed, if $f(0) \neq 0$, then $f(1)$ has the opposite sign, implying a root in $(0, 1)$ by continuity, and if $f(0) = 0$, then $\alpha = 0$ is a root.

To get an explicit expression for $f(\alpha)$, suppose first that $0 < \alpha < 1$ and rewrite (14) as

$$f(\alpha) = \frac{1}{2\pi i} \int_\Gamma k \frac{\lambda e^{ik(1-\alpha)} - e^{ik\alpha}}{\mathcal{L}(k, c)} dk - \frac{1}{2\pi i} \int_\Gamma k \frac{\lambda e^{-ik(1-\alpha)} - e^{-ik\alpha}}{\mathcal{L}(k, c)} dk.$$

Since $\alpha > 0$ and $1 - \alpha > 0$, we can close the contour in the first integral by a semi-arch at infinity in the upper half of the complex plane and the contour in the second integral in the lower half plane and apply Jordan's lemma and residue theorem to each of the resulting integrals. Recalling from the above discussion that the contour Γ goes above the real roots of $\mathcal{L}(k,c)$ with $c_g < c$ (the set $N_-(c)$) and below the roots with $c_g > c$ (the set $N_+(c)$) and that the contour also goes above $k = 0$, we then obtain

$$f(\alpha) = \sum_{k \in M^+(c)} k \frac{\lambda e^{ik(1-\alpha)} - e^{ik\alpha}}{\mathcal{L}_k(k,c)} + \sum_{k \in M^-(c)} k \frac{\lambda e^{-ik(1-\alpha)} - e^{-ik\alpha}}{\mathcal{L}_k(k,c)} + \frac{\lambda - 1}{\lambda - 2(1+\lambda)c^2}, \qquad 0 < \alpha < 1. \tag{15}$$

Here

$$M_\pm = \{k : \ \mathcal{L}(k,c) = 0, \ \mathrm{Im} k \gtrless 0\} \cup N_\pm$$

are the sets of (generally complex) roots included in the corresponding closed contours.

If $-1 < \alpha < 0$, we write (14) as

$$f(\alpha) = \frac{1}{2\pi i} \int_\Gamma k \frac{\lambda e^{ik(1-\alpha)} + e^{-ik\alpha}}{\mathcal{L}(k,c)} dk - \frac{1}{2\pi i} \int_\Gamma k \frac{\lambda e^{-ik(1-\alpha)} + e^{ik\alpha}}{\mathcal{L}(k,c)} dk.$$

and again close the contours in the first and second integrals in the upper and lower half planes, respectively, and apply Jordan's lemma, which holds because $\alpha < 0$ and $1 - \alpha > 0$ now. This yields

$$f(\alpha) = \sum_{k \in M^+(c)} k \frac{\lambda e^{ik(1-\alpha)} + e^{-ik\alpha}}{\mathcal{L}_k(k,c)} + \sum_{k \in M^-(c)} k \frac{\lambda e^{-ik(1-\alpha)} + e^{ik\alpha}}{\mathcal{L}_k(k,c)} + \frac{\lambda + 1}{\lambda - 2(1+\lambda)c^2}, \qquad -1 < \alpha < 0. \tag{16}$$

One can show that the expressions (15), (16) yield the same limit as $\alpha \to 0$ and thus describe a continuous function on the interval $-1 < \alpha < 1$.

The problem thus reduces to finding the roots of $\mathcal{L}(k,c)$ for given c and then solving $f(\alpha) = 0$ in the interval $(-1,1)$; note that in general there may be more than one solution. For each α we then find the corresponding solutions (12), which can also be written in terms of residues. The resulting

expressions (31-33) and (36-38) are presented in the Appendix. They imply the following relation between the average strains at $\pm\infty$:

$$w_- = w_+ + \frac{1}{1-(c/c_s)^2}, \tag{17}$$

where

$$c_s = \sqrt{\frac{\lambda}{2(\lambda+1)}} \tag{18}$$

has the physical meaning of half the macroscopic sound speed, as we shall see below. Since $w_- > w_+$ under our assumptions, (17) implies that the phase boundary must be subsonic: $c < c_s$. We also obtain the following relation between the strains $w_\pm$ at infinity and c (see Appendix for details):

$$\begin{aligned} w_\pm = w_c &\mp \frac{1}{2(1-(c/c_s)^2)} \\ &+ \frac{1}{2}\Bigg(\sum_{k\in N_-(c)} \frac{c^2k^2(\lambda+1-e^{ik(\alpha-1)}(\lambda+e^{ik}))-4\lambda\sin^2\frac{k}{2}}{k\mathcal{L}_k(k,c)} \\ &- \sum_{k\in N_+(c)} \frac{c^2k^2(\lambda+1-e^{ik(\alpha-1)}(\lambda+e^{ik}))-4\lambda\sin^2\frac{k}{2}}{k\mathcal{L}_k(k,c)} \Bigg). \end{aligned} \tag{19}$$

For given $c > 0$ and for each of the corresponding roots α of (15), (16) the formal solution is thus furnished by (31-33) and (36-38). If the inequalities (8) are satisfied, it is an admissible solution of the traveling wave problem.

We now consider the limiting cases. At $\lambda = 1$ (equal masses) we have

$$\mathcal{L}(k,c) = c^4k^4 + 4\sin^2\frac{k}{2} - 4c^2k^2 = \left(c^2k^2 - 4\cos^2\frac{k}{4}\right)\left(c^2k^2 - 4\sin^2\frac{k}{4}\right). \tag{20}$$

Meanwhile, $\alpha = 0.5$ clearly satisfies $f(\alpha) = 0$ in this case (there may be other roots). With this value of α, the numerators in the integrands of (12) in the expressions for $r(\xi)$ and $s(\xi)$ both become $4\sin^2\frac{k}{4}(c^2k^2 - 4\cos^2\frac{k}{4})$. Thus the factor $c^2k^2 - 4\cos^2\frac{k}{4}$ in the numerator and denominator cancels out, and we obtain

$$\begin{aligned} r(\xi) &= w_+ + \frac{1}{2\pi i}\int_\Gamma \frac{4\sin^2\frac{k}{4}}{k(c^2k^2 - 4\sin^2\frac{k}{4})} e^{ik\xi}dk \\ s(\xi) &= w_+ + \frac{1}{2\pi i}\int_\Gamma \frac{4\sin^2\frac{k}{4}}{k(c^2k^2 - 4\sin^2\frac{k}{4})} e^{ik(\xi+1/2)}dk. \end{aligned} \tag{21}$$

If we now let $w_n(t) = r_{n/2}(t) = r(n/2 - ct)$ if n is even and $w_n(t) = s_{(n-1)/2}(t) = s((n-1)/2 - ct)$ if n is odd, we can write $w = w(\zeta)$, $\zeta = n - Vt$, $V = 2c$. Replacing $k/2$ by k in the integral, we obtain

$$w(\zeta) = w_+ + \frac{1}{2\pi i} \int_\Gamma \frac{4 \sin^2 \frac{k}{2}}{k(V^2 k^2 - 4 \sin^2 \frac{k}{2})} e^{ik\zeta} dk,$$

thus recovering the solution in [39, 46, 47]. The solution can also be written in terms of plane waves using residue theorem and Jordan's lemma as in the Appendix.

In the limit $\lambda \to 0$ ($M \gg m$ for fixed m), the sound speed (18) tends to zero, and since the phase boundary velocity must be subsonic, there are no traveling wave solutions with nonzero velocity in this case. Recall that in this case the dimer cells become uncoupled, and thus a signal cannot propagate through the chain.

Stationary states. Another important limit is $c = 0$, when a phase boundary becomes stationary. Seeking equilibrium solutions of (1), we have $f(r_n) = f(s_n) = \sigma$ for all n, where σ is the stress in the chain. Due to bilinear nonlinearity this means $r_n = s_n = \sigma + 1 > w_c$ for springs in phase II and $r_n = s_n = \sigma < w_c$ for springs in phase I. The solution thus exists and is stable in the *trapping region* $w_c - 1 < \sigma < w_c$, i.e. while all the springs remain in their respective phases. At the boundaries of the trapping region, such solutions cease to exist, and a phase boundary propagation or nucleation is initiated.

Shock solutions. In addition to phase transition fronts we constructed above, there are traveling wave fronts connecting the uniform equilibrium states in the same phase. These solutions describe a shock wave propagating through the linear chain with average velocity equal to the sound speed $V_s = 2c_s$. Shock solutions in a semi-infinite linear diatomic chain under a velocity impact at the end were derived and analyzed in [31].

4 Connection to the macroscopic problem and the kinetic relation

The simplest continuum approximation of the system (1) is the partial differential equation, which after rescaling takes the form

$$\frac{1}{V_s^2}u_{tt} = (f(u_x))_x, \tag{22}$$

where we recall that $V_s = 2c_s$ is the sound speed in each phase and

$$\frac{1}{V_s^2} = \frac{\lambda+1}{2\lambda}$$

thus yields the rescaled density on the continuum level. The phase boundary in this limit is represented by a moving discontinuity. Recall that the Rankine-Hugoniot jump conditions for the strain $w = u_x$ and the particle velocity $\nu = u_t$ across a discontinuity moving with velocity V are

$$\frac{V^2}{V_s^2}[\![w]\!] = [\![f(w)]\!], \qquad [\![\nu]\!] = -V[\![w]\!], \tag{23}$$

where $[\![g]\!] = g_+ - g_-$ denotes the jump of g. In addition to the above jump conditions, the continuum theory requires that the rate of energy dissipation must be nonnegative: $\mathcal{R} = GV \geq 0$. Here

$$G = [\![\phi(w)]\!] - \{f\}[\![w]\!] = \frac{w_+ + w_-}{2} - w_c \tag{24}$$

is the configurational (driving) force, with $\phi(w) = \int f(w)dw$ being the energy density and $\{f\} = (f(w_+) - f(w_-))/2$ denoting the average stress across the discontinuity. In case of subsonic discontinuities ($V < V_s$), which violate the Lax condition, this is, however, not sufficient to obtain a unique solution of the initial value problem associated with (22) [12, 26, 36, 45]. To see this, consider (22) with piecewise constant Riemann initial data $u_x(x,0) = w_L\theta(-x)$, $u_t(x,0) = 0$ prescribed on the real line, with given constant initial left strain $w_L > 0$. The structure of an expected piecewise constant solution is shown in Fig. 2. It features a phase boundary propagating with velocity $V < V_s$ and two shock waves propagating away from it. There are five unknowns: w_-, w_+, ν_-, ν_+ and V. However, there are only four jump

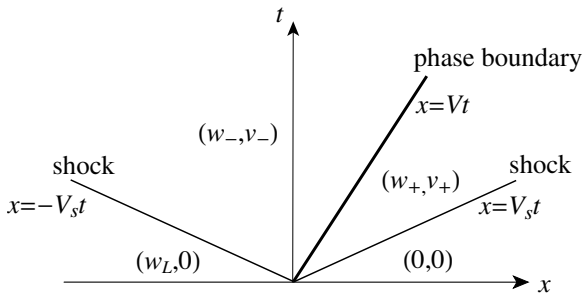

Figure 2: Solution of the continuum problem with a single propagating phase boundary.

conditions: two across the phase boundary and one across each shock (since shocks propagate with $V = \pm V_s$, the first of (23) is trivially satisfied). Thus, we obtain a one-parameter family of solutions. To remove this unphysical non-uniqueness and provide the needed closure of the continuum problem, (22) must be supplemented by a *kinetic relation* $G = G(V)$ specifying the dependence of the configurational force on the velocity of the phase boundary [1, 44]. Classical continuum theory provides no information about phase boundary kinetics.

As shown in [47] (see also [39, 48, 43, 49]) for the case of monatomic chain ($\lambda = 1$), the missing kinetic relation can be obtained from the underlying discrete model. Indeed, the traveling wave solution we obtained for the discrete problem replaces the discontinuity by a transition layer (core region). The solution features non-decaying oscillations about the average values $w_\pm$, with wave numbers $k \in N_\pm(V/2)$, which are due to the lattice waves (phonons) emitted by the moving front. These waves carry energy away from the moving front, resulting in what is perceived on the macroscopic level as energy dissipation. Observe also that the first jump condition in (23) coincides with the condition (17) we obtained in the discrete problem. The second jump condition can be similarly recovered after solving for the particle velocity [47]. In the continuum limit, the width of the transition layer goes to zero, but the kinetic information is *retained* in the relations (19) between the strains

$w_\pm$ and $c = V/2$. Together with (24) they imply the kinetic relation

$$G(V) = \frac{1}{2}\Bigg(\sum_{k \in N_-(V/2)} \frac{\frac{V^2}{4}k^2(\lambda + 1 - e^{-i\alpha k}(\lambda + e^{ik})) - 4\lambda \sin^2 \frac{k}{2}}{k\mathcal{L}_k(k, V/2)} - \sum_{k \in N_+(V/2)} \frac{\frac{V^2}{4}k^2(\lambda + 1 - e^{-i\alpha k}(\lambda + e^{ik})) - 4\lambda \sin^2 \frac{k}{2}}{k\mathcal{L}_k(k, V/2)} \Bigg). \tag{25}$$

Alternatively, the same kinetic relation can be obtained by computing the fluxes of energy carried by the emitted lattice waves [47].

Note that the trapping region $w_c - 1 < \sigma < w_c$ for stationary states ($V = 0$) corresponds to $|G| < 1/2$. This means that a phase boundary may remain trapped in the lattice until the magnitude of driving force reaches the Peierls value $G_P = 1/2$ (though there may be dynamic solutions coexisting with the stationary ones, as we shall see). Beyond this value, only dynamic solutions are possible.

5 The root structure

We now return to the discrete problem and consider the structure of the nonzero roots of $\mathcal{L}(k, c)$, which, as we recall, determines the traveling wave solution.

Note that (13) can be written as

$$\mathcal{L}(k, c) = k^4(g^2(k) - c^2)(h^2(k) - c^2),$$

where

$$g(k) = \frac{\sqrt{\lambda + 1 + \sqrt{(\lambda + 1)^2 - 4\lambda \sin^2(k/2)}}}{|k|}$$
$$h(k) = \frac{\sqrt{\lambda + 1 - \sqrt{(\lambda + 1)^2 - 4\lambda \sin^2(k/2)}}}{|k|} \tag{26}$$

correspond to the two branches of the dispersion curve. Note that $g(k) \geq h(k)$ for $\lambda \leq 1$ and that a strict inequality holds when $\lambda < 1$. Observe also that the value of $h(k)$ at $k = 0$, which is also its maximum value, equals the half sound speed (18). At a given $c > 0$ the nonzero real roots thus solve

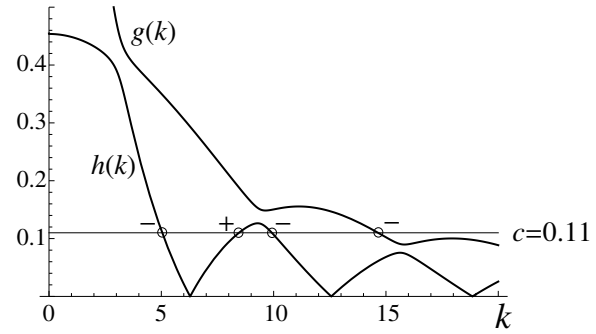

Figure 3: The functions $g(k)$ and $h(k)$ at $\lambda = 0.7$ and the corresponding real roots at $c = 0.11$. Pluses and minuses mark the roots in the sets N_+ and N_-, respectively.

$g(k) = c$ and $h(k) = c$, with $c_g \gtrless c$ if $g'(k) \gtrless 0$ and $h'(k) \gtrless 0$, respectively. This means that the sets of real roots are given by

$$N_\pm(c) = \{k:\ g(k) = c,\ g'(k) \gtrless 0\} \cup \{k:\ h(k) = c,\ h'(k) \gtrless 0\}.$$

Fig. 3 shows $g(k)$ and $h(k)$ and the corresponding positive real roots at $c = 0.11$ and $\lambda = 0.7$. The values of c corresponding to extrema of $g(k)$ and $h(k)$ are resonance velocities; observe that the constructed solutions (31-33), (36-38) are not defined at such c since $\mathcal{L}_k(k, c) = 0$ in the denominator.

In addition to the real roots, there are infinitely many complex roots with nonzero imaginary part, which contribute to the structure of the core region around the phase boundary. Branches of these roots bifurcate from the branches of real roots in the space $(\mathrm{Re}k, \mathrm{Im}k, c)$ as shown in Fig. 4. Specifically, unbounded branches of complex roots, shown in red, bifurcate from the local maxima of $g(k)$. Additional branches, shown in green, bifurcate from the local maxima of $h(k)$. Each of these branches either terminates at the nearest local minimum of $g(k)$ or, when there is no such minimum nearby (lower λ), is unbounded.

As $\lambda \to 1$, the branches $g(k)$ and $h(k)$ of the real roots become closer. At $\lambda = 1$ the local minima of $g(k)$ coincide with local maxima of $h(k)$ at nonzero k; recall that in this case $\mathcal{L}(k, c)$ can be factorized as in (20). In the other limiting case, $\lambda = 0$, the acoustic branch of the dispersion relation disappears ($h(k) = 0$), and the optical branch yields $g(k) = \sqrt{2}/|k|$.

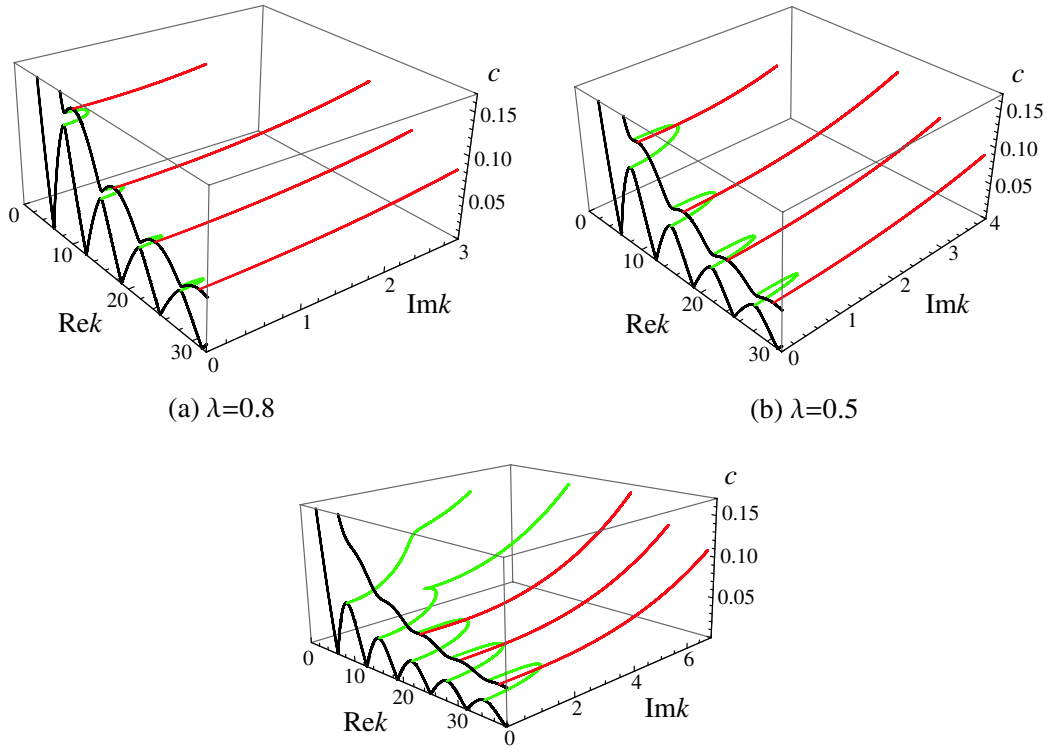

(a) λ=0.8

(b) λ=0.5

(c) λ=0.2

Figure 4: Nonzero roots of $\mathcal{L}(k, c)$ at different λ. The real roots are in black, and the other roots are in red and green.

6 Strain profiles and kinetic relation: some examples

We now consider some examples of strain profiles and kinetic relation corresponding to the constructed traveling wave solutions. The procedure for obtaining solutions was as follows. For given $c > 0$ and $0 < \lambda < 1$, we computed the first N roots of $\mathcal{L}(k, c)$ (typically, $N = 400$) and found roots α in $(-1, 1)$ of the function $f(\alpha)$ defined in (15), (16). For each value of α, we then found w_+ and w_- using (19), we calculated the corresponding driving force (25) and computed the solutions $r(\xi)$ and $s(\xi)$. Since the continuity of the solution (31-33) and (36-38) at $\xi = 0$ and $\xi = -\alpha$, respectively, requires the condition (34), which is not satisfied exactly when only finitely many roots are taken into account, we computed $r(\xi)$ at $|\xi| \leq 0.5$ and $s(\xi)$ at $|\xi + \alpha| \leq 0.5$ numerically using (12) with small added viscosity to remove singularities from the real axis. For ξ outside these neighborhoods, (31-33) and (36-38) were used.

As an example, consider $c = 0.2$ and $\lambda = 0.8$. In this case there are two positive real roots, one solving $h(k) = c$ and the other $g(k) = c$. Both roots are along the decreasing portions of the corresponding functions and thus belong to $N_-(c)$, while $N_+(c)$ is empty. After finding other roots and substituting the resulting sets into (15), (16), we find that there are five solutions of $f(\alpha) = 0$ in the $(-1, 1)$ interval: $\alpha = 0.5008$, 0.0395, 0.0006, -0.0687 and -0.4592. Of these, only $\alpha = 0.5008$ yields an admissible solution, i.e. a solution which satisfies the assumed inequalities (8). The corresponding profiles of $r(\xi)$ and $s(\xi)$ are shown in Fig. 5a. There are constant-amplitude lattice waves propagating behind the moving front due the real roots in $N_-(c)$. The combination of oscillations with two different wave numbers results in a weakly quasi-periodic structure. There are no lattice waves moving ahead of the phase boundary because $N_+(c)$ is empty. Meanwhile, all other roots lead to non-admissible strain profiles, which violate the assumed inequalities (8) by intersecting the line $w = w_c$ more than once and thus must be discarded. See, for example, $r(\xi)$ (solid line) in the inset of Fig. 5b ($\alpha = -0.4592$).

At $\lambda = 0.5$ and $\lambda = 0.2$, there are two admissible solutions for each λ at $c = 0.2$, corresponding to $\alpha > 0$ and $\alpha < 0$ and shown in Fig. 5c-f. In particular, the solutions in (d) and (f) have $\alpha < 0$ and are admissible, while the corresponding root at $\lambda = 0.8$ did not yield an admissible strain profile for $r(\xi)$ (see (b)). Recall that solutions at $\alpha > 0$ correspond to the s-springs

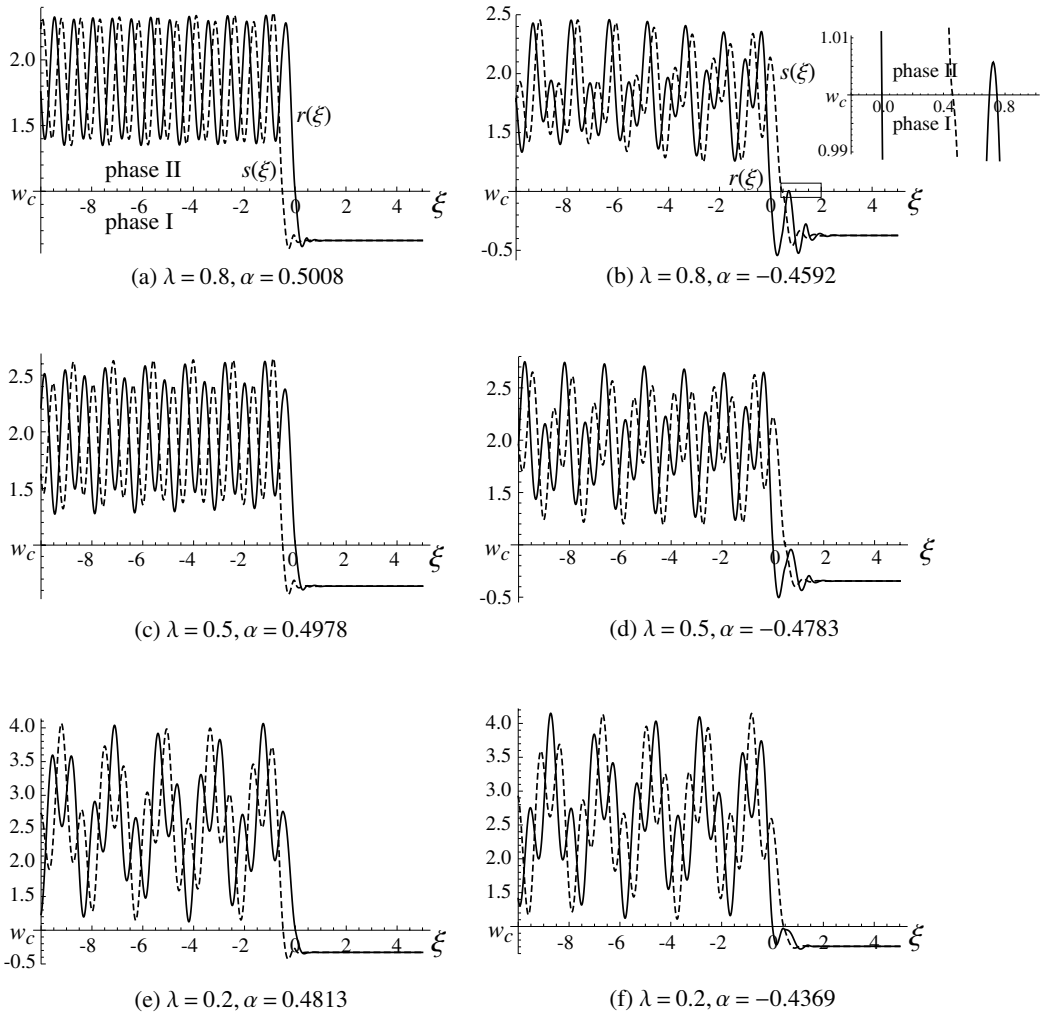

Figure 5: Strain profiles $r(\xi)$ (solid line) and $s(\xi)$ (dashed line) at $c = 0.2$, $w_c = 1$ and different λ and α. The profiles in (a), (c-f) are admissible solutions, while (b) violates the inequalities (8). Inset in (b) zooms in on the rectangle near $\xi = 0$.

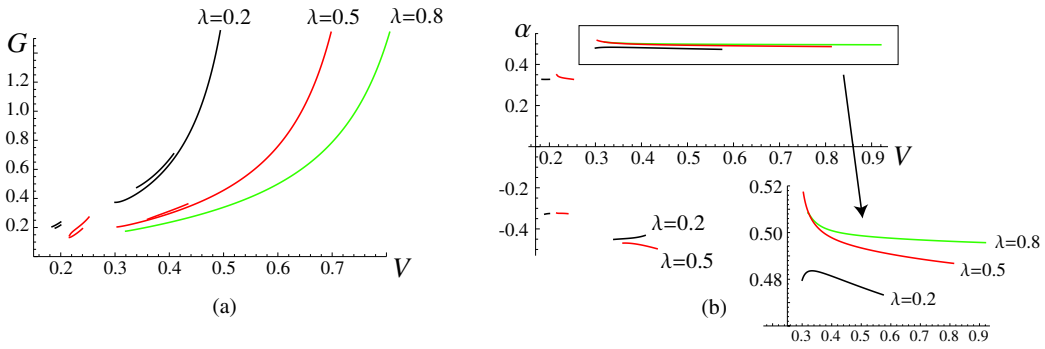

Figure 6: (a) The kinetic relation $G(V)$ and (b) the corresponding $\alpha(V)$ for $\lambda = 0.2$ (black segments), $\lambda = 0.5$ (red) and $\lambda = 0.8$ (green) at $V \geq 0.15$. Only branches containing solutions that are admissible at $w_c = 1$ are shown.

switching phase after the r-springs behind them in a dimer cell, while $\alpha < 0$ means that an s-spring in each (r, s) cell will change phase first.

Our results suggest that for each λ there are velocity intervals at small enough c in which the formally constructed solution violates the assumed inequalities (8) for all possible values of α. This means that solutions satisfying (8) do not exist in these velocity intervals, whose structure depends on w_c. It should be noted, however, that the assumptions (7) and (8) are too restrictive. For example, in a closely related Frenkel-Kontorova model with the same bilinear nonlinearity it is possible to construct admissible solutions that equal the critical value over an interval of ξ values, rather than a single point, at velocities below the first resonance [34]; similar calculations can also be done in this case. However, such solutions are likely to be unstable, and we will not pursue this issue further in this paper.

Fig. 6 shows the kinetic relation (25) at $V = 2c \geq 0.15$ and the corresponding $\alpha(V)$ for which admissible solutions were found at $w_c = 1$. Observe that as λ decreases, a higher driving force is needed to propagate a phase transition front at the same velocity, due to the weaker coupling between dimer cells. Note also that while solutions with $\alpha > 0$ are dominant, at smaller values of λ there are velocity intervals where they coexist with solutions that have $\alpha < 0$. The new type of solutions with $\alpha < 0$ is thus a consequence of lattice heterogeneity and has no analog in a uniform chain. At sufficiently high velocities, there is only one root, $\alpha > 0$. As V approaches the sound speed limit $2c_s$, the driving force tends to infinity, and α tends to

a limiting value that depends on λ.

7 Stability of the obtained solutions

To test stability of the obtained solutions we conducted numerical simulations of the system (2) with bilinear nonlinearity (6) on a finite chain with n_f masses (typically $n_f = 600$), solving for $w_n(t)$ such that $w_n = r_{n/2}$ if n is even and $w_n = s_{(n-1)/2}$ if n is odd. Two types of initial conditions were considered. The first had piecewise constant strain

$$w_n(0) = \begin{cases} w_L, & n < n_0 \\ w_c, & n = n_0 \\ 0, & n > n_0, \end{cases} \tag{27}$$

while in the second a smooth initial strain was prescribed:

$$w_n(0) = w_L\left(1 - \frac{1}{2}\tanh(n - n_0)\right). \tag{28}$$

In both cases $n_0 = n_f/2$, and the initial particle velocity was zero, so $\dot{w}_n(0) = 0$. We chose $w_L > w_c > 0$, so that the initial condition had a phase boundary at $n = n_0$. The left strain w_L served as the control parameter. The boundary conditions in the numerical simulations were consistent with the initial data: $w_0 = w_L$ and $w_{n_f} = 0$. Each simulation was run until long-time behavior could be determined (typically $t = 300$). The length of the chain was chosen so that there is no wave reflection from the boundaries during the simulation time, and the symplectic Verlet algorithm was used.

Typical results with both types of initial conditions are as follows. At w_L below a certain threshold the long-time solution features a stationary phase boundary, with two shocks propagating away from it with the average speed $V_s = 2c_s$. At higher w_L one of the two possible scenarios happens. In one, the initial interface starts propagating but after some time multiple new phase boundaries nucleate (see Fig. 7). In another scenario, after an initial transient time interval the solution approaches a limit in which a steady phase transition wave propagates to the right and two shocks are moving away from it. As the wave propagates, dimer cells consisting of a consecutive pair of even-numbered (r-spring) and odd-numbered (s-spring) springs change from phase I to phase II. In some cases (see also further discussion below), the

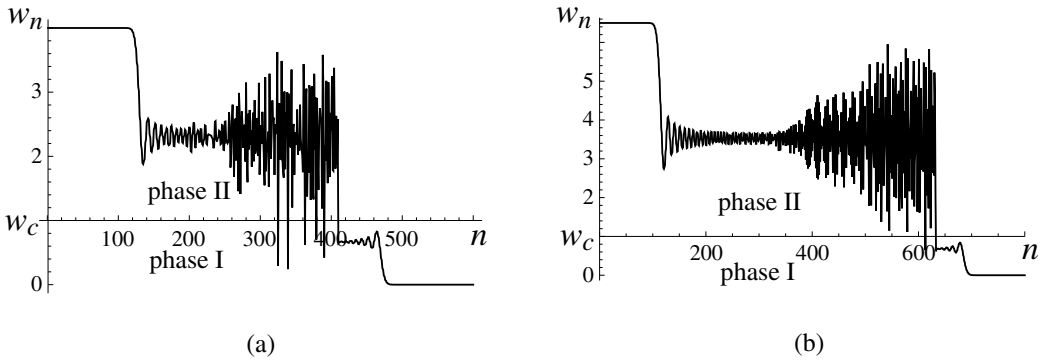

Figure 7: Snapshots of strain profiles exhibiting multiple phase boundaries in numerical simulations with Riemann initial data (27) at $w_c = 1$, $\lambda = 0.2$ and (a) $w_L = 4.0$, $t = 300$; (b) $w_L = 6.5$, $t = 500$.

s-spring in each dimer cell changes phase before the r-spring. Typically, however, the r-spring switches phase first, so that the springs in the chain change phase one after another. Fig. 8a shows an example of such a solution with the initial conditions (27) at $\lambda = 0.5$, $t = 300$ and $w_L = 2.7$. During the simulation, we tracked the displacement $x_p(t)$ of the phase boundary from the initial position (defined at each t as $n - n_0$ such that $w_n(t) > w_c$ and $w_{n+1}(t) < w_c$) and measured the time intervals T between phase switching times of consecutive springs. The results are shown in Fig. 8c. One can see that at large t these intervals oscillate between alternating smaller and higher values, which in this case are 2.9 and 5.78. This is consistent with the constructed traveling wave solutions for even and odd-numbered strains: recall that there is a time delay between the times when even and odd springs switch phase. The average phase boundary velocity resulting from the simulations is thus $V = 0.23$ yielding $c = V/2 = 0.115$ for even/odd springs. Fig. 8b compares the numerical solution (circles) around the phase boundary to the corresponding strain profile obtained from the analytical solution (solid line). The good agreement between the two indicates stability of the constructed traveling wave solution.

For a more systematic comparison of numerical and analytical solutions in the parameter range leading to a steady phase transition wave, consider the solution of the continuum problem (22), (23) with the piecewise constant initial data specified above. Recall that the solution on the macroscopic level is piecewise constant, as shown in Fig. 2. As in the numerical simulation

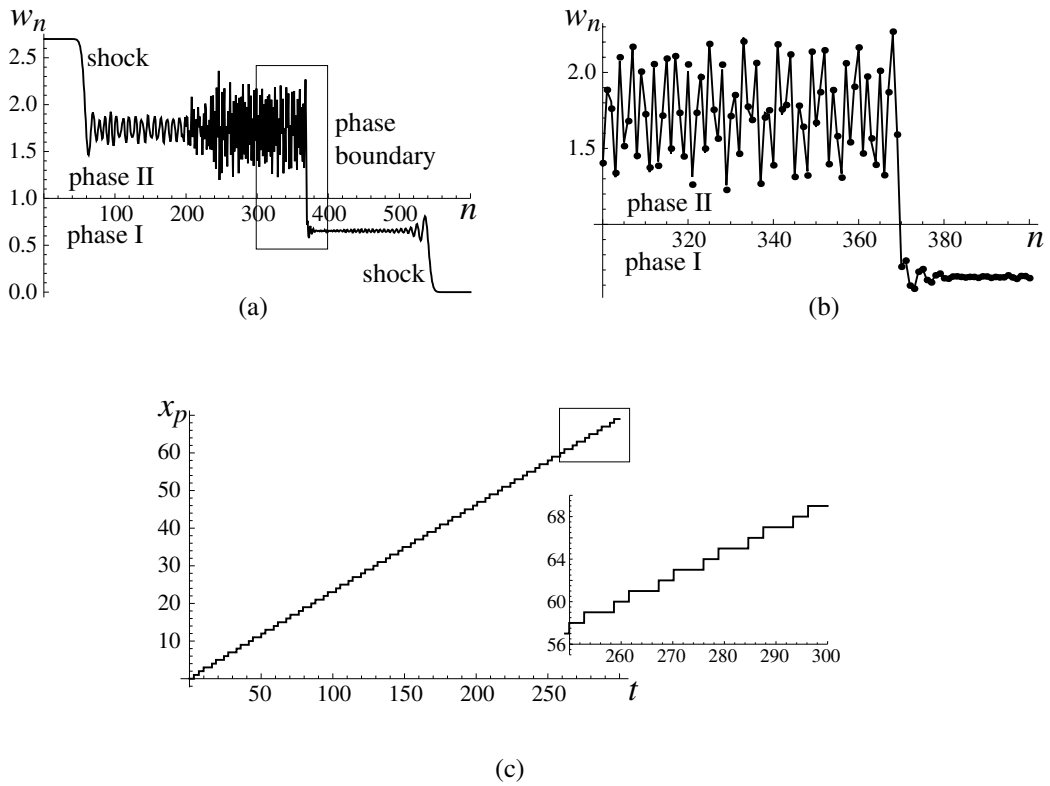

Figure 8: (a) The results of numerical simulations with Riemann initial data (27) at $t = 300$, with $w_c = 1$, $\lambda = 0.5$ and $w_L = 2.7$. The average velocity of the phase boundary is $V = 0.23$. (b) Numerical solution (circles) zoomed-in around the phase boundary and compared to the analytical solution (solid line) at $c = V/2$ and $\alpha = 0.3342$. (c) The displacement $x_p(t)$ of the phase boundary from its initial position. Inset: zoom in on the region inside the rectangle.

described above, there is a subsonic phase boundary moving with velocity $V = 2c$ and two shocks moving away from it with the sound speed $V_s = 2c_s$. Recall that to obtain a unique solution of the continuum problem we must supplement it by a kinetic relation $G = G(V)$. This relation is "hidden" in the discrete problem which does not need any additional conditions to generate a unique solution. Rather than use (25), the relation we obtained from the traveling wave solution, we will extract the kinetic relation from the numerical solution of the discrete problem, and compare the two. Using the jump conditions (23) across the two shocks and the phase boundary and recalling that $G = (w_+ + w_-)/2 - w_c$, we obtain

$$G = \frac{w_L}{2} - \frac{V}{2V_s(1 - (V/V_s)^2)} - w_c. \tag{29}$$

If the numerical simulation for a given w_L generates a long-time solution that corresponds to a single phase boundary on the macrolevel, we can calculate its average speed V at large t (averaged over the last ten time intervals), compute the driving force (29) and compare the result to the analytical kinetic relation.

The results are shown in Fig. 9 and Fig. 10, with (V, G) pairs obtained from solutions with a single macroscopic phase boundary that were generated for different w_L from piecewise constant initial strain (27) (red circles) and smooth initial data (28) (green circles). Traveling wave solutions selected by the initial data (and thus apparently stable) have velocities in certain intervals ($[0.438, 0.453]$ at $\lambda = 0.2$, $[0.225, 0.247]$ and $[0.34, 0.6]$ at $\lambda = 0.5$ and $[0.329, 0.71]$ at $\lambda = 0.8$), with the corresponding ranges of w_L. Initial data with w_L outside these ranges lead to long-time numerical solutions that either feature a stationary phase boundary (small enough w_L, $V = 0$) or have multiple phase boundaries as in Fig. 7. It is important to remark, however, that traveling wave solutions that are not selected are not necessarily unstable since they may have a narrow basin of attraction which does not include the initial data considered here.

Note, in particular, that numerical simulations suggest stability of some traveling wave solutions with $\alpha < 0$ at $\lambda = 0.5$ when the driving force is sufficiently small; see Fig. 9b. Recall that in these solutions the s-spring in each (r, s) cell changes phase first, thus temporarily creating three phase boundaries instead of a single one on the microlevel. Once the r-spring changes phase, there is again a single interface, until the s-spring in the next cell transforms, and so on. This is illustrated in Fig. 11 which shows evolution

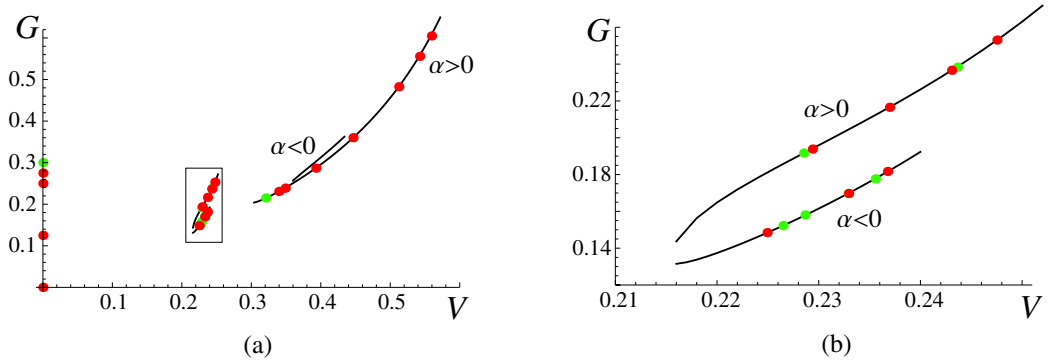

Figure 9: (a) Comparison of the kinetic relation obtained from the numerical simulations (circles) to the analytical relation (25) at $\lambda = 0.5$ and $w_c = 1$. (b) Zoomed-in rectangle in (b). Only branches of (25) corresponding to admissible traveling wave solutions are shown. Red and green circles indicate numerical simulations corresponding to initial conditions (27) and (28), respectively.

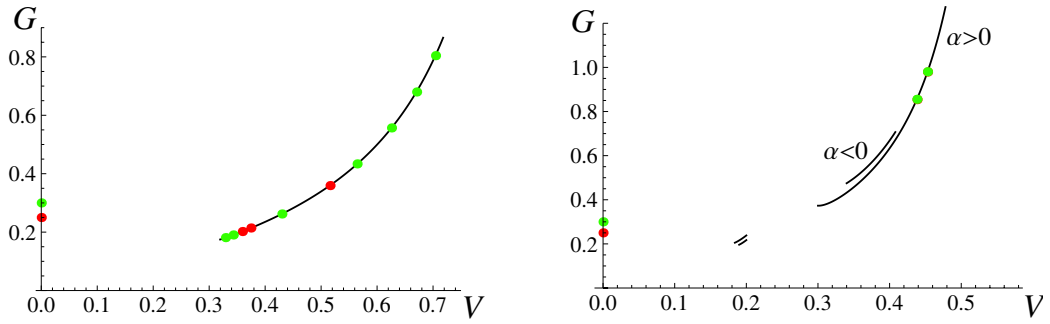

Figure 10: Comparison of the kinetic relation obtained from the numerical simulations (circles) to the analytical relation (25) at $\lambda = 0.8$ and $\lambda = 0.2$, with $w_c = 1$. Red and green circles indicate numerical simulations corresponding to initial conditions (27) and (28), respectively.

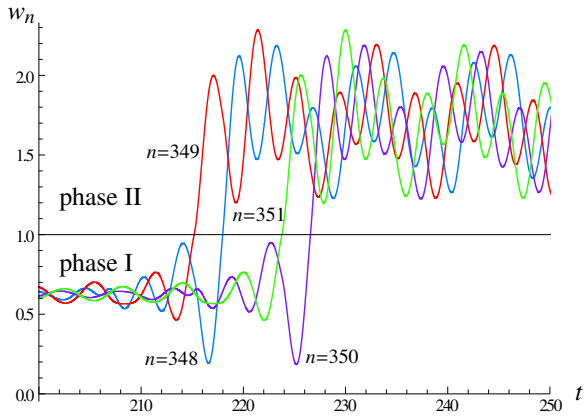

Figure 11: Strain evolution in the numerical solution with initial data (28), $\lambda = 0.5$, $w_c = 1$ at $w_L = 2.65$, which corresponds to $V = 0.233$ and $\alpha = -0.325$.

of the strains in two neighboring cells, $(w_{348}, w_{349}) = (r_{174}(t), s_{174}(t))$ and $(w_{350}, w_{351}) = (r_{175}(t), s_{175}(t))$ for a solution with $\alpha < 0$. On the macroscopic level, these details are averaged out, and there is only one phase boundary, which in this case propagates with a slightly higher velocity, $V = 0.233$, than in the solution with $\alpha > 0$ ($\alpha = 0.66$, $V = 0.221$) and the same driving force, $G = 0.17$.

Observe also that apparently stable solutions corresponding to different α and different driving force may coexist at the same velocity, and that steady motion at different velocities (including stationary ones) and different α may coexist at the same value of the driving force. Finally, note that at smaller λ the range of driving forces where the constructed traveling wave solutions are selected by the initial data becomes more narrow, and higher driving forces are required due to the weaker coupling between dimer cells.

8 Some additional numerical experiments and ensuing waveforms

Traveling phase transition and shock waves moving at constant average speed are not the sole waveforms that arise in this dimer chain. In this section, we briefly give some examples of another type of waveform that may arise

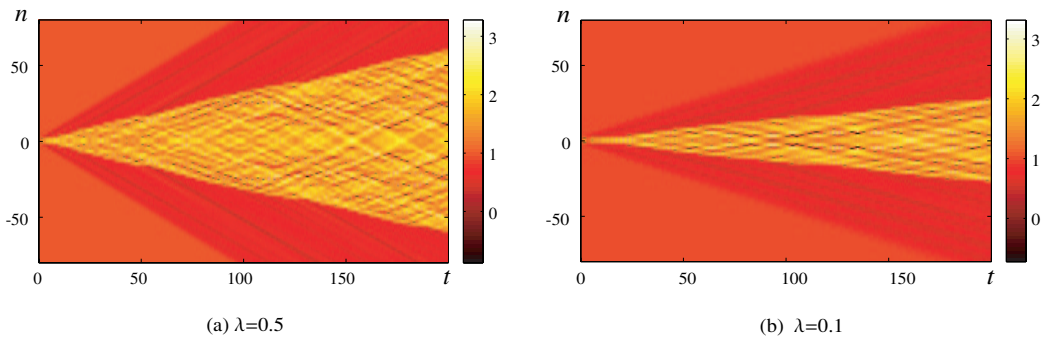

(a) λ=0.5 (b) λ=0.1

Figure 12: Space (n)-time (t) contour plot of the field w_n initialized below the critical point $w_c = 1$ by 10^{-4}, while the central site is above the critical point by 10^{-4}. A twinkling phase spontaneously emerges as a result in the dimer chain with (a) $\lambda = 0.5$ and (b) $\lambda = 0.1$.

in the dynamics (spontaneously so) to provide a feeling about the additional wealth of phenomenology inherent in the model.

Motivated by the work of [3, 4], we have initialized the chain with all the sites being very close to the critical point (of $w_c = 1$) but slightly below it, while a single site is slightly supercritical (by around 10^{-4}). The results are shown in Fig. 12 and Fig. 13. We see that this initial condition produces in addition to the outgoing shock waves an oscillatory structure whereby in each cycle each of the participating sites crosses the critical point (as it goes from yellow to red, or from grayer to darker) once. This is the so-called twinkling phase analyzed in detail for a monatomic chain [3, 4], and it is certainly a dynamical behavior also available in the dimer case. Focusing on the differences of this twinkling phase from its monomer analog of $\lambda = 1$, we note that as observed in [3, 4], in the latter case, the phase remains nearly periodic for a number of periods (about 10), and then becomes random. In the dimer case of Fig. 13, we observe that this periodicity is almost lost and both the size of the regions in each phase (phase I or II) within the twinkling phase and their dynamics appears to be random. Another aspect in which the twinkling phase is affected in the dimer chain is controlled by the magnitude of λ. The effect here is somewhat similar to what we observed in the traveling waves discussed previously. Namely, as λ is decreased, the effective connectivity between the dimer pairs is reduced and thus the progressive expansion of the twinkling phase is slowed down (and of course the corresponding shock waves

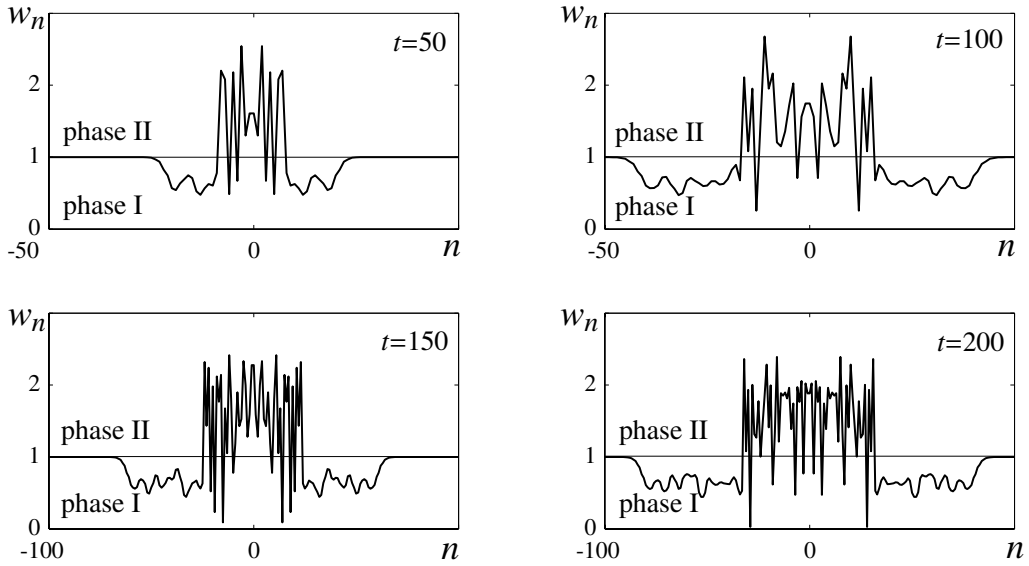

Figure 13: Snapshots of strain profiles corresponding to the simulation in Fig. 12a with $\lambda = 0.5$.

formed at its edges are slower too). This is seen by comparing the results for $\lambda = 0.5$ and $\lambda = 0.1$ in Fig. 12.

9 Conclusions and future challenges

In the present work, we have considered the case of a dimer chain with one of the arguably simplest possible forms of nonlinearity, namely a piecewise linear interaction modeling phase transitions. This enables an analytical description of heteroclinic traveling wave solutions representing a subsonic phase transition front propagating through the chain. The solution is obtained using Fourier transform and determined by the roots of the linear part of the traveling wave problem. These roots were identified for different values of the fundamental parameters of the system such as the speed c and the ratio of the masses λ and were used in order to explicitly construct the corresponding traveling waves. We showed that the resulting kinetic relation between the driving force on the phase boundary and its velocity is strongly dependent on λ. In particular, as λ decreases, the sound speed becomes smaller, and

a higher driving force is required to propagate the phase boundary through the chain at the given speed. This is the result of the progressively weaker coupling of dimer cells as $\lambda \to 0$. A key feature in the diatomic case $\lambda < 1$ is that the kinetic relation may become multivalued, as a given velocity value may correspond to more than one values of the parameter α, which measures the delay between the times the two springs in a dimer cell switch phases, and thus more than one value of the driving force. In particular, the two springs may change phase in different order, resulting in a new type of solution that is only seen when λ is sufficiently small.

Stability of the resulting waves was partially investigated via direct numerical simulations. The results suggest stability of the constructed solutions in some velocity intervals. At intermediate values of λ and sufficiently small driving force, the results suggest coexistence of two stable traveling wave solutions (i.e. bistability) differing by the order in which the springs change phase within a dimer cell. A glimpse was also given of a different type of waveform that may (even spontaneously) arise in this simplified yet fairly rich paradigm of a dynamical lattice, such as the twinkling phases.

A number of interesting questions, however, still remain open in connection to this model. For example, we showed a twinkling phase that bears some similarities to its analog in the single component model, but it would be interesting to examine whether there are such solutions in the dimer with no single component counterpart. On the other hand, determining whether some form of breather excitation (i.e. exponentially localized in space and periodic in time) may arise in this model would be of particular value in its own right. Despite our efforts (from both an analytical and numerical perspective), we have not yet identified such solutions within this model, however, it would be interesting to offer a definitive answer to this question as well. Additional interesting aspects could involve the consideration of non-nearest-neighbor interactions in the spirit of [46, 47] and the examination of the interplay of their strength (or of their relative strength to nearest-neighbor ones) with the role of the mass ratio λ explored herein. Finally, it would also be useful to consider the case of trilinear interactions, as in the work of [49]. This enables the formation of a non-degenerate spinodal region and should introduce interesting additional ramifications to the diatomic model. Results of such studies will be reported in future publications.

Acknowledgments. This work was supported by the NSF grants DMS-1007908 (A.V.), DMS-0806762 and CMMI-1000337, as well as by the Alexan-

der von Humboldt Foundation and the Alexander S. Onassis Public Benefit Foundation (P.G.K.).

Appendix

In this Appendix, we derive explicit expressions for $r(\xi)$ and $s(\xi)$. Observe that $r(\xi)$ in (12) can be written as

$$\begin{aligned} r(\xi) =& w_+ + \frac{1}{2\pi i}\int\limits_{\Gamma} \frac{c^2k^2(\lambda+1)-4\lambda\sin^2\frac{k}{2}}{k\mathcal{L}(k,c)}e^{ik\xi}dk \\ &- \frac{\lambda c^2}{2\pi i}\int\limits_{\Gamma}\frac{k}{\mathcal{L}(k,c)}e^{ik(\xi+\alpha-1)}dk - \frac{c^2}{2\pi i}\int\limits_{\Gamma}\frac{k}{\mathcal{L}(k,c)}e^{ik(\xi+\alpha)}dk \end{aligned} \tag{30}$$

Closing the contour of integration by semi-arches at infinity in the upper (lower) half plane for $\xi > 0$ ($\xi < 0$) in the first integral, $\xi > 1-\alpha$ ($\xi < 1-\alpha$) in the second and $\xi > -\alpha$ ($\xi < -\alpha$) in the third and applying the residue theorem and Jordan's lemma, we then obtain the exact solution for $r(\xi)$ given by

$$r(\xi) = w_+ + \begin{cases} \displaystyle\sum_{k\in M_+(c)} \frac{c^2k^2(\lambda+1-e^{ik(\alpha-1)}(\lambda+e^{ik}))-4\lambda\sin^2\frac{k}{2}}{k\mathcal{L}_k(k,c)}e^{ik\xi}, & \xi \geq 1-\alpha \\ \displaystyle\sum_{k\in M_+(c)} \frac{c^2k^2(\lambda+1-e^{ik\alpha}-4\lambda\sin^2\frac{k}{2}}{k\mathcal{L}_k(k,c)}e^{ik\xi} + \frac{\lambda c^2}{\lambda-2(\lambda+1)c^2} + \lambda c^2\sum_{k\in M_-(c)}\frac{ke^{ik(\xi+\alpha-1)}}{\mathcal{L}_k(k,c)}, & 0 < \xi \leq 1-\alpha \\ \displaystyle\sum_{k\in M_+(c)} \frac{c^2k^2(\lambda+1-e^{ik\alpha}-4\lambda\sin^2\frac{k}{2}}{k\mathcal{L}_k(k,c)} + \frac{\lambda c^2}{\lambda-2(\lambda+1)c^2} + \lambda c^2\sum_{k\in M_-(c)}\frac{ke^{ik(\alpha-1)}}{\mathcal{L}_k(k,c)} + \frac{1}{2}, & \xi = 0+ \\ \displaystyle\frac{\lambda-c^2}{\lambda-2(\lambda+1)c^2} - c^2\sum_{k\in M_+(c)}\frac{ke^{ik\alpha}}{\mathcal{L}_k(k,c)} - \sum_{k\in M_-(c)}\frac{c^2k^2(\lambda+1-\lambda e^{ik(\alpha-1)}))-4\lambda\sin^2\frac{k}{2}}{k\mathcal{L}_k(k,c)} - \frac{1}{2}, & \xi = -0 \\ \displaystyle\frac{\lambda-c^2}{\lambda-2(\lambda+1)c^2} - c^2\sum_{k\in M_+(c)}\frac{ke^{ik(\xi+\alpha)}}{\mathcal{L}_k(k,c)} - \sum_{k\in M_-(c)}\frac{c^2k^2(\lambda+1-\lambda e^{ik(\alpha-1)}))-4\lambda\sin^2\frac{k}{2}}{k\mathcal{L}_k(k,c)} - \frac{1}{2}, & -\alpha \leq \xi < 0 \\ \displaystyle\frac{\lambda}{\lambda-2(\lambda+1)c^2} - \sum_{k\in M_-(c)}\frac{c^2k^2(\lambda+1-e^{ik(\alpha-1)}(\lambda+e^{ik}))-4\lambda\sin^2\frac{k}{2}}{k\mathcal{L}_k(k,c)}e^{ik\xi}, & \xi \leq -\alpha. \end{cases} \tag{31}$$

for $0 < \alpha < 1$,

$$r(\xi) = w_+ +$$

$$\begin{cases} \sum\limits_{k\in M_+(c)} \dfrac{\lambda c^2k^2(1-e^{-ik}) - 4\lambda\sin^2\frac{k}{2}}{k\mathcal{L}_k(k,c)}e^{ik\xi}, & \xi \geq 1 \\ \sum\limits_{k\in M_+(c)} \dfrac{\lambda c^2k^2 - 4\lambda\sin^2\frac{k}{2}}{k\mathcal{L}_k(k,c)}e^{ik\xi} + \dfrac{\lambda c^2}{\lambda - 2(\lambda+1)c^2} + \lambda c^2 \sum\limits_{k\in M_-(c)} \dfrac{ke^{ik(\xi-1)}}{\mathcal{L}_k(k,c)}, & 0 < \xi \leq 1 \\ \sum\limits_{k\in M_+(c)} \dfrac{\lambda c^2k^2 - 4\lambda\sin^2\frac{k}{2}}{k\mathcal{L}_k(k,c)} + \dfrac{\lambda c^2}{\lambda - 2(\lambda+1)c^2} + \lambda c^2 \sum\limits_{k\in M_-(c)} \dfrac{ke^{-ik}}{\mathcal{L}_k(k,c)} + \dfrac{1}{2}, & \xi = 0+ \\ \dfrac{\lambda}{\lambda - 2(\lambda+1)c^2} - \sum\limits_{k\in M_-(c)} \dfrac{\lambda c^2k^2(1-e^{-ik}) - 4\lambda\sin^2\frac{k}{2}}{k\mathcal{L}_k(k,c)} - \dfrac{1}{2}, & \xi = -0 \\ \dfrac{\lambda}{\lambda - 2(\lambda+1)c^2} - \sum\limits_{k\in M_-(c)} \dfrac{\lambda c^2k^2(1-e^{-ik}) - 4\lambda\sin^2\frac{k}{2}}{k\mathcal{L}_k(k,c)}e^{ik\xi}, & \xi < 0. \end{cases} \tag{32}$$

for $\alpha = 0$ and

$$r(\xi) = w_+ +$$

$$\begin{cases} \sum\limits_{k\in M_+(c)} \dfrac{c^2k^2(\lambda+1-e^{ik(\alpha-1)}(\lambda+e^{ik})) - 4\lambda\sin^2\frac{k}{2}}{k\mathcal{L}_k(k,c)}e^{ik\xi}, & \xi \geq 1-\alpha \\ \sum\limits_{k\in M_+(c)} \dfrac{c^2k^2(\lambda+1-e^{ik\alpha} - 4\lambda\sin^2\frac{k}{2}}{k\mathcal{L}_k(k,c)}e^{ik\xi} + \dfrac{\lambda c^2}{\lambda - 2(\lambda+1)c^2} + \lambda c^2 \sum\limits_{k\in M_-(c)} \dfrac{ke^{ik(\xi+\alpha-1)}}{\mathcal{L}_k(k,c)}, & -\alpha \leq \xi \leq 1-\alpha \\ \sum\limits_{k\in M_+(c)} \dfrac{c^2k^2(\lambda+1) - 4\lambda\sin^2\frac{k}{2}}{k\mathcal{L}_k(k,c)}e^{ik\xi} + \dfrac{(\lambda+1)c^2}{\lambda - 2(\lambda+1)c^2} + c^2 \sum\limits_{k\in M_-(c)} \dfrac{k(\lambda+e^{ik})e^{ik(\xi+\alpha-1)}}{\mathcal{L}_k(k,c)}, & 0 < \xi \leq -\alpha \\ \sum\limits_{k\in M_+(c)} \dfrac{c^2k^2(\lambda+1) - 4\lambda\sin^2\frac{k}{2}}{k\mathcal{L}_k(k,c)} + \dfrac{(\lambda+1)c^2}{\lambda - 2(\lambda+1)c^2} + c^2 \sum\limits_{k\in M_-(c)} \dfrac{k(\lambda+e^{ik})e^{ik(\alpha-1)}}{\mathcal{L}_k(k,c)} + \dfrac{1}{2}, & \xi = +0 \\ \dfrac{\lambda}{\lambda - 2(\lambda+1)c^2} - \sum\limits_{k\in M_-(c)} \dfrac{c^2k^2(\lambda+1-e^{ik(\alpha-1)}(\lambda+e^{ik})) - 4\lambda\sin^2\frac{k}{2}}{k\mathcal{L}_k(k,c)} - \dfrac{1}{2}, & \xi = -0 \\ \dfrac{\lambda}{\lambda - 2(\lambda+1)c^2} - \sum\limits_{k\in M_-(c)} \dfrac{c^2k^2(\lambda+1-e^{ik(\alpha-1)}(\lambda+e^{ik})) - 4\lambda\sin^2\frac{k}{2}}{k\mathcal{L}_k(k,c)}e^{ik\xi}, & \xi < 0. \end{cases} \tag{33}$$

for $-1 < \alpha < 0$.

Note that the contribution of the first integral in (30) along the semi-arches at infinity is $\pm 1/2$ when $\xi = \pm 0$. This is the result of model degeneracy which can be removed by taking interactions of longer range into account [47]. Observe that continuity of the solution at $\xi = 0$ is ensured by the fact that the sum of all residues at $\xi = 0$ equals negative one (the contribution at infinity), or

$$\sum_{k\in M(c)} \frac{c^2k^2(\lambda+1) - 4\lambda\sin^2\frac{k}{2}}{k\mathcal{L}_k(k,c)} - \frac{(\lambda+1)c^2}{\lambda - 2(\lambda+1)c^2} = 0. \tag{34}$$

Here $M(c) = M_+(c) \cup M_-(c)$.

Together with the switch condition $r(0) = w_c$, $f(\alpha) = 0$ and (17), the continuity implies the relation (19) between the strains $w_\pm$ at infinity and c. Here we used the fact that the sums of the complex roots in $M_\pm(c)$ cancel out due to the following symmetry property: if $k \in M_+(c)\backslash N_+(c)$, then $-k \in M_-(c)\backslash N_-(c)$. Meanwhile, for real roots, if $k \in N_+(c)$, then $-k \in N_+(c)$ (similarly for N_-), and thus only the sums over real roots enter (19).

The explicit solution for $s(\xi)$ is found in a similar way. In this case we write

$$\begin{aligned} s(\xi) =& w_+ + \frac{1}{2\pi i}\int\limits_\Gamma \frac{c^2k^2(\lambda+1) - 4\lambda\sin^2\frac{k}{2}}{k\mathcal{L}(k,c)}e^{ik(\xi+\alpha)}dk \\ &- \frac{\lambda c^2}{2\pi i}\int\limits_\Gamma \frac{k}{\mathcal{L}(k,c)}e^{ik(\xi+1)}dk - \frac{c^2}{2\pi i}\int\limits_\Gamma \frac{k}{\mathcal{L}(k,c)}e^{ik\xi}dk \end{aligned} \tag{35}$$

and obtain

$$s(\xi) = w_+ + \begin{cases} \displaystyle\sum_{k\in M_+(c)} \frac{c^2k^2(\lambda+1-e^{ik(1-\alpha)}(\lambda+e^{-ik})) - 4\lambda\sin^2\frac{k}{2}}{k\mathcal{L}_k(k,c)}e^{ik(\xi+\alpha)}, & \xi \geq 0 \\ \displaystyle\frac{c^2}{\lambda-2(\lambda+1)c^2} + c^2\sum_{k\in M_-(c)}\frac{ke^{ik\xi}}{\mathcal{L}_k(k,c)} + \sum_{k\in M_+(c)}\frac{c^2k^2(1+\lambda(1-e^{ik(1-\alpha)})) - 4\lambda\sin^2\frac{k}{2}}{k\mathcal{L}_k(k,c)}e^{ik(\xi+\alpha)}, & -\alpha < \xi \leq 0 \\ \displaystyle\frac{c^2}{\lambda-2(\lambda+1)c^2} + c^2\sum_{k\in M_-(c)}\frac{ke^{-ik\alpha}}{\mathcal{L}_k(k,c)} + \sum_{k\in M_+(c)}\frac{c^2k^2(1+\lambda(1-e^{ik(1-\alpha)})) - 4\lambda\sin^2\frac{k}{2}}{k\mathcal{L}_k(k,c)} + \frac{1}{2}, & \xi = -\alpha + 0 \\ \displaystyle\frac{\lambda(1-c^2)}{\lambda-2(\lambda+1)c^2} - \sum_{k\in M_-(c)}\frac{c^2k^2(\lambda+1-e^{-ik\alpha}) - 4\lambda\sin^2\frac{k}{2}}{k\mathcal{L}_k(k,c)} - \lambda c^2\sum_{k\in M_+(c)}\frac{ke^{ik(1-\alpha)}}{\mathcal{L}_k(k,c)} - \frac{1}{2}, & \xi = -\alpha - 0 \\ \displaystyle\frac{\lambda(1-c^2)}{\lambda-2(\lambda+1)c^2} - \sum_{k\in M_-(c)}\frac{c^2k^2(\lambda+1-e^{-ik\alpha}) - 4\lambda\sin^2\frac{k}{2}}{k\mathcal{L}_k(k,c)}e^{ik(\xi+\alpha)} - \lambda c^2\sum_{k\in M_+(c)}\frac{ke^{ik(\xi+1)}}{\mathcal{L}_k(k,c)}, & -1 \leq \xi < -\alpha \\ \displaystyle\frac{\lambda}{\lambda-2(\lambda+1)c^2} - \sum_{k\in M_-(c)}\frac{c^2k^2(\lambda+1-e^{ik(1-\alpha)}(\lambda+e^{-ik})) - 4\lambda\sin^2\frac{k}{2}}{k\mathcal{L}_k(k,c)}e^{ik(\xi+1)}, & \xi \leq -1. \end{cases} \tag{36}$$

for $0 < \alpha < 1$,

$s(\xi) = w_+ +$

$$\begin{cases} \displaystyle\sum_{k\in M_+(c)} \frac{c^2k^2(\lambda(1-e^{ik}) - 4\lambda\sin^2\frac{k}{2}}{k\mathcal{L}_k(k,c)} e^{ik\xi}, & \xi > 0 \\ \displaystyle\sum_{k\in M_+(c)} \frac{c^2k^2(\lambda(1-e^{ik}) - 4\lambda\sin^2\frac{k}{2}}{k\mathcal{L}_k(k,c)} + \frac{1}{2}, & \xi = +0 \\ \displaystyle\frac{\lambda(1-c^2)}{\lambda - 2(\lambda+1)c^2} - \sum_{k\in M_-(c)} \frac{\lambda c^2k^2 - 4\lambda\sin^2\frac{k}{2}}{k\mathcal{L}_k(k,c)} - \lambda c^2 \sum_{k\in M_+(c)} \frac{ke^{ik}}{\mathcal{L}_k(k,c)} - \frac{1}{2}, & \xi = -0 \\ \displaystyle\frac{\lambda(1-c^2)}{\lambda - 2(\lambda+1)c^2} - \sum_{k\in M_-(c)} \frac{\lambda c^2k^2(\lambda+1) - 4\lambda\sin^2\frac{k}{2}}{k\mathcal{L}_k(k,c)} e^{ik\xi} - \lambda c^2 \sum_{k\in M_+(c)} \frac{ke^{ik(\xi+1)}}{\mathcal{L}_k(k,c)}, & -1 \le \xi < 0 \\ \displaystyle\frac{\lambda}{\lambda - 2(\lambda+1)c^2} - \sum_{k\in M_-(c)} \frac{c^2k^2(\lambda(1-e^{ik}) - 4\lambda\sin^2\frac{k}{2}}{k\mathcal{L}_k(k,c)} e^{ik\xi}, & \xi \le -1. \end{cases} \tag{37}$$

for $\alpha = 0$ and

$s(\xi) = w_+ +$

$$\begin{cases} \displaystyle\sum_{k\in M_+(c)} \frac{c^2k^2(\lambda+1-e^{ik(1-\alpha)}(\lambda+e^{-ik})) - 4\lambda\sin^2\frac{k}{2}}{k\mathcal{L}_k(k,c)} e^{ik(\xi+\alpha)}, & \xi > -\alpha \\ \displaystyle\sum_{k\in M_+(c)} \frac{c^2k^2(\lambda+1-e^{ik(1-\alpha)}(\lambda+e^{-ik})) - 4\lambda\sin^2\frac{k}{2}}{k\mathcal{L}_k(k,c)} + \frac{1}{2}, & \xi = -\alpha + 0 \\ \displaystyle\frac{\lambda - (\lambda+1)c^2}{\lambda - 2(\lambda+1)c^2} - \sum_{k\in M_-(c)} \frac{c^2k^2(\lambda+1) - 4\lambda\sin^2\frac{k}{2}}{k\mathcal{L}_k(k,c)} - c^2 \sum_{k\in M_+(c)} \frac{k(\lambda+e^{-ik})e^{ik(1-\alpha)}}{\mathcal{L}_k(k,c)} - \frac{1}{2}, & \xi = -\alpha - 0 \\ \displaystyle\frac{\lambda - (\lambda+1)c^2}{\lambda - 2(\lambda+1)c^2} - \sum_{k\in M_-(c)} \frac{c^2k^2(\lambda+1) - 4\lambda\sin^2\frac{k}{2}}{k\mathcal{L}_k(k,c)} e^{ik(\xi+\alpha)} - c^2 \sum_{k\in M_+(c)} \frac{k(\lambda+e^{-ik})e^{ik(\xi+1)}}{\mathcal{L}_k(k,c)}, & 0 \le \xi < -\alpha \\ \displaystyle\frac{\lambda(1-c^2)}{\lambda - 2(\lambda+1)c^2} - \sum_{k\in M_-(c)} \frac{c^2k^2(\lambda+1-e^{-ik\alpha}) - 4\lambda\sin^2\frac{k}{2}}{k\mathcal{L}_k(k,c)} e^{ik(\xi+\alpha)} - \lambda c^2 \sum_{k\in M_+(c)} \frac{ke^{ik(\xi+1)}}{\mathcal{L}_k(k,c)}, & -1 \le \xi \le 0 \\ \displaystyle\frac{\lambda}{\lambda - 2(\lambda+1)c^2} - \sum_{k\in M_-(c)} \frac{c^2k^2(\lambda+1-e^{ik(1-\alpha)}(\lambda+e^{-ik})) - 4\lambda\sin^2\frac{k}{2}}{k\mathcal{L}_k(k,c)} e^{ik(\xi+\alpha)}, & \xi \le -1. \end{cases} \tag{38}$$

for $-1 < \alpha < 0$. Note that the continuity at $\xi = -\alpha$ follows from (34). Together with the switch condition $s(-\alpha) = w_c$ and (17) it again yields (19).

References

[1] R. Abeyaratne and J.K. Knowles. Kinetic relations and the propagation of phase boundaries in solids. *Arch. Rat. Mech. Anal.*, 114:119–154, 1991.

[2] W. Atkinson and N. Cabrera. Motion of a Frenkel-Kontorova dislocation in a one-dimensional crystal. *Phys. Rev. A*, 138(3):763–766, 1965.

[3] A. M. Balk, A. V. Cherkaev, and L. I. Slepyan. Dynamics of chains with non-monotone stress-strain relations-I. model and numerical experiments. *J. Mech. Phys. Solids*, 49:131–148, 2001.

[4] A. M. Balk, A. V. Cherkaev, and L. I. Slepyan. Dynamics of chains with non-monotone stress-strain relations-II. nonlinear waves and waves of phase transition. *J. Mech. Phys. Solids*, 49:149–171, 2001.

[5] H. Bilz, H. Büttner, A. Bussmann-Holder, W. Kress, and U. Schröder. Nonlinear lattice dynamics of crystals with structural phase transitions. *Phys. Rev. Lett.*, 48(4):264–267, Jan 1982.

[6] N. Boechler, G. Theocharis, S. Job, P.G. Kevrekidis, Mason A. Porter, and C. Daraio. Discrete breathers in one-dimensional diatomic granular crystals. *Physical Review Letters*, 104:244302, 2010.

[7] L. Brillouin. *Wave propagation in periodic structures.* Dover, New York, 1953.

[8] David K. Campbell, Phillip Rosenau, and George Zaslavsky. Introduction: The Fermi-Pasta-Ulam problem—The first fifty years. *Chaos*, 15(1):015101, 2005.

[9] A. Carpio and L. L. Bonilla. Depinning transitions in discrete reaction-diffusion equations. *SIAM J. Appl. Math.*, 63(3):1056–1082, 2003.

[10] A. Carpio and L. L. Bonilla. Oscillatory wave fronts in chains of coupled nonlinear oscillators. *Phys. Rev. E*, 67:056621, 2003.

[11] V. Celli and N. Flytzanis. Motion of a screw dislocation in a crystal. *J. Appl. Phys.*, 41(11):4443–4447, 1970.

[12] C. M. Dafermos. *Hyperbolic conservation laws in continuum physics.* Springer Verlag, Heidelberg, 2000.

[13] Y. Y. Earmme and J. H. Weiner. Dislocation dynamics in the modified Frenkel-Kontorova model. *J. Appl. Phys.*, 48(8):3317–3331, 1977.

[14] G. Fáth. Propagation failure of traveling waves in discrete bistable medium. *Physica D*, 116:176–190, 1998.

[15] J. Fleischer, G. Bartal, O. Cohen, T. Schwartz, O. Manela, B. Freedman, M. Segev, H. Buljan, and N. Efremidis. Spatial photonics in nonlinear waveguide arrays. *Optics Express*, 13(6):1780–1796, 2005.

[16] N. Flytzanis. The dynamics of a diatomic chain on a parabolic substrate. *Phys. Let. A*, 85(6-7):353–355, 1981.

[17] N. Flytzanis, V. Celli, and A. Nobile. Motion of two screw dislocations in a lattice. *J. Appl. Phys.*, 45(12):5176–5181, 1974.

[18] N. Flytzanis, S. Crowley, and V. Celli. High velocity dislocation motion and interatomic force law. *J. Phys. Chem. Solids*, 38:539–552, 1977.

[19] Joseph Ford. The Fermi-Pasta-Ulam problem: Paradox turns discovery. *Physics Reports*, 213(5):271–310, 1992.

[20] S. Ishioka. Uniform motion of a screw dislocation in a lattice. *J. Phys. Soc. Jpn.*, 30:323–327, 1971.

[21] G. James and M. Kastner. Bifurcations of discrete breathers in a diatomic fermi-pasta-ulam chain. *Nonlinearity*, 20(3):631–657, 2007.

[22] Yuri S. Kivshar and Govind P. Agrawal. *Optical Solitons: From Fibers to Photonic Crystals.* Academic Press, San Diego, California, 2003.

[23] O. Kresse and L. Truskinovsky. Mobility of lattice defects: discrete and continuum approaches. *J. Mech. Phys. Solids*, 51:1305–1332, 2003.

[24] O. Kresse and L. Truskinovsky. Lattice friction for crystalline defects: from dislocations to cracks. *J. Mech. Phys. Solids*, 52:2521–2543, 2004.

[25] A. Lahiri, S. Panda, and T. K. Roy. Discrete breathers: exact solutions in piecewise linear models. *Phys. Rev. Lett.*, 84(16):3570–3573, 2000.

[26] P. G. LeFloch. *Hyperbolic systems of conservation laws.* ETH Lecture Note Series. Birkhouser, 2002.

[27] R. Livi, M. Spicci, and R.S. MacKay. Breathers on a diatomic fpu chain. *Nonlinearity*, 10(6):1421–1434, 1997.

[28] M. Marder and S. Gross. Origin of crack tip instabilities. *J. Mech. Phys. Solids*, 43:1–48, 1995.

[29] G. S. Mishuris, A. B. Movchan, and L. I. Slepyan. Localization and dynamic defects in lattice structures. In V. V. Silberschmidt, editor, *Computational and experimental mechanics of advanced materials*, volume 514 of *CISM Courses and Lectures*, pages 51–82. Springer, 2009.

[30] O. Morsch and M. Oberthaler. Dynamics of bose-einstein condensates in optical lattices. *Reviews of Modern Physics*, 78(1):179–215, 2006.

[31] M. J. P. Musgrave and J. Tasi. Shock waves in diatomic chains - I. Linear analysis. *J. Mech. Phys. Solids*, 24:19–42, 1976.

[32] Michel Peyrard. Nonlinear dynamics and statistical physics of DNA. *Nonlinearity*, 17:R1–R40, 2004.

[33] M. J. Rice and E. J. Mele. Elementary excitations of a linearly conjugated diatomic polymer. *Phys. Rev. Lett.*, 49(19):1455–1459, Nov 1982.

[34] P. Rosakis and A. Vainchtein, 2011. In preparation.

[35] M. Sato, B. E. Hubbard, and A. J. Sievers. *Colloquium*: Nonlinear energy localization and its manipulation in micromechanical oscillator arrays. *Reviews of Modern Physics*, 78:137, 2006.

[36] D. Serre. *Systems of conservation laws*, volume 1, 2. Cambridge University Press, Cambridge, 1999.

[37] L. I. Slepyan. Dynamics of a crack in a lattice. *Sov. Phys. Dokl.*, 26(5):538–540, 1981.

[38] L. I. Slepyan. *Models and phenomena in Fracture Mechanics*. Springer-Verlag, New York, 2002.

[39] L. I. Slepyan, A. Cherkaev, and E. Cherkaev. Transition waves in bistable structures. II. Analytical solution: wave speed and energy dissipation. *J. Mech. Phys. Solids*, 53:407–436, 2005.

[40] L. I. Slepyan and L. V. Troyankina. Fracture wave in a chain structure. *J. Appl. Mech. Tech. Phys.*, 25(6):921–927, 1984.

[41] L. I. Slepyan and L. V. Troyankina. Impact waves in a nonlinear chain. In R. V. Gol'dstein, editor, *Plasticity and fracture of solids*, pages 175–186. Nauka, Moscow, 1988. (in Russian).

[42] Andrey A. Sukhorukov and Yuri S. Kivshar. Discrete gap solitons in modulated waveguide arrays. *Optics Letters*, 27(23):2112–2114, 2002.

[43] E. Trofimov and A. Vainchtein. Kinks vs shocks in a discrete model of displacive phase transitions. *Cont. Mech. Thermodyn.*, 22(5):317–344, 2010.

[44] L. Truskinovsky. Dynamics of nonequilibrium phase boundaries in a heat conducting elastic medium. *J. Appl. Math. Mech.*, 51:777–784, 1987.

[45] L. Truskinovsky. Kinks versus shocks. In E. Dunn R. Fosdick and M. Slemrod, editors, *Shock Induced Transitions and Phase Structures in General Media*, volume 52 of *IMA*, pages 185–229. Springer-Verlag, 1993.

[46] L. Truskinovsky and A. Vainchtein. Explicit kinetic relation from "first principles". In P. Steinmann and G.A. Maugin, editors, *Mechanics of Material Forces*, pages 43–50. Springer, 2005.

[47] L. Truskinovsky and A. Vainchtein. Kinetics of martensitic phase transitions: Lattice model. *SIAM J. Appl. Math.*, 66:533–553, 2005.

[48] L. Truskinovsky and A. Vainchtein. Dynamics of martensitic phase boundaries: discreteness, dissipation and inertia. *Cont. Mech. Thermodyn.*, 20(2):97–122, 2008.

[49] A. Vainchtein. The role of spinodal region in the kinetics of lattice phase transitions. *J. Mech. Phys. Solids*, 58(2):227–240, 2009.

[50] A. Vainchtein. Effect of nonlinearity on the steady motion of a twinning dislocation. *Physica D*, 239:1170–1179, 2010.

[51] A. Vainchtein and E. S. Van Vleck. Nucleation and propagation of phase mixtures in a bistable chain. *Phys. Rev. B*, 79(14):144123, 2009.

[52] Y. Zhen and A. Vainchtein. Dynamics of steps along a martensitic phase boundary I: Semi-analytical solution. *J. Mech. Phys. Solids*, 56(2):496–520, 2008.

[53] Y. Zhen and A. Vainchtein. Dynamics of steps along a martensitic phase boundary II: Numerical simulations. *J. Mech. Phys. Solids*, 56(2):521–541, 2008.